

Alternating Current Photovoltaic Effect

Haiyang Zou, Guozhang Dai, Aurelia Chi Wang, Xiaogan Li, Steven L. Zhang, Wenbo Ding, Lei Zhang, Ying Zhang, and Zhong Lin Wang*

It is well known that the photovoltaic effect produces a direct current (DC) under solar illumination owing to the directional separation of light-excited charge carriers at the p–n junction, with holes flowing to the p-side and electrons flowing to the n-side. Here, it is found that apart from the DC generated by the conventional p–n photovoltaic effect, there is another new type of photovoltaic effect that generates alternating current (AC) in the nonequilibrium states when the illumination light periodically shines at the junction/interface of materials. The peak current of AC at high switching frequency can be much higher than that from DC. The AC cannot be explained by the established mechanisms for conventional photovoltaics; instead, it is suggested to be a result of the relative shift and realignment between the quasi-Fermi levels of the semiconductors adjacent to the junction/interface under the nonequilibrium conditions, which results in electron flow in the external circuit back and forth to balance the potential difference between two electrodes. By virtue of this effect, the device can work as a high-performance broadband photodetector with extremely high sensitivity under zero bias; it can also work as a remote power source providing extra power output in addition to the conventional photovoltaic effect.

It is highly desirable to discover renewable and clean energy for the sustainable development of human civilization.^[1,2] Photovoltaic (PV) has been widely investigated in solar cells as a sustainable energy source to replace fossil fuels.^[3] The conventional photovoltaic effect based on p–n junction model converts light energy directly into electricity via processes of light absorption, carrier excitation, hole/electron separation, charge transport, and recombination.^[4–6] Owing to the separation of the holes and electrons by a built-in potential at the junction/interface, it naturally provides a direct current (DC) output. There are some other mechanisms to generate voltage and current in a material upon exposure to light. The Dember effect is generated when

photoexcited electrons and holes have different mobilities; thus, there is a potential difference between the illuminated and nonilluminated areas in a homogeneous limited semiconductor.^[7,8] A single crystal with a noncentrosymmetric structure exhibits the bulk photovoltaic effect that under uniform illumination, an anomalously large photovoltage originates from the different probabilities for photoexcited carrier motion in one direction versus the opposite direction, caused by the absence of centrosymmetry in the material.^[9,10] Photoelectric current can also be produced by photon-drag effect, that the momentum carried by electromagnetic waves is transferred to the charge carriers during interband or intraband energy transitions, leading to the ordered motion of the carriers relative to the lattice in the direction of light propagation.^[11,12] Becquerel photovoltaic effect has also been explored at a semiconductor–electrolyte interface for the conversion of radiant energy to electrical

and/or chemical energy.^[13]

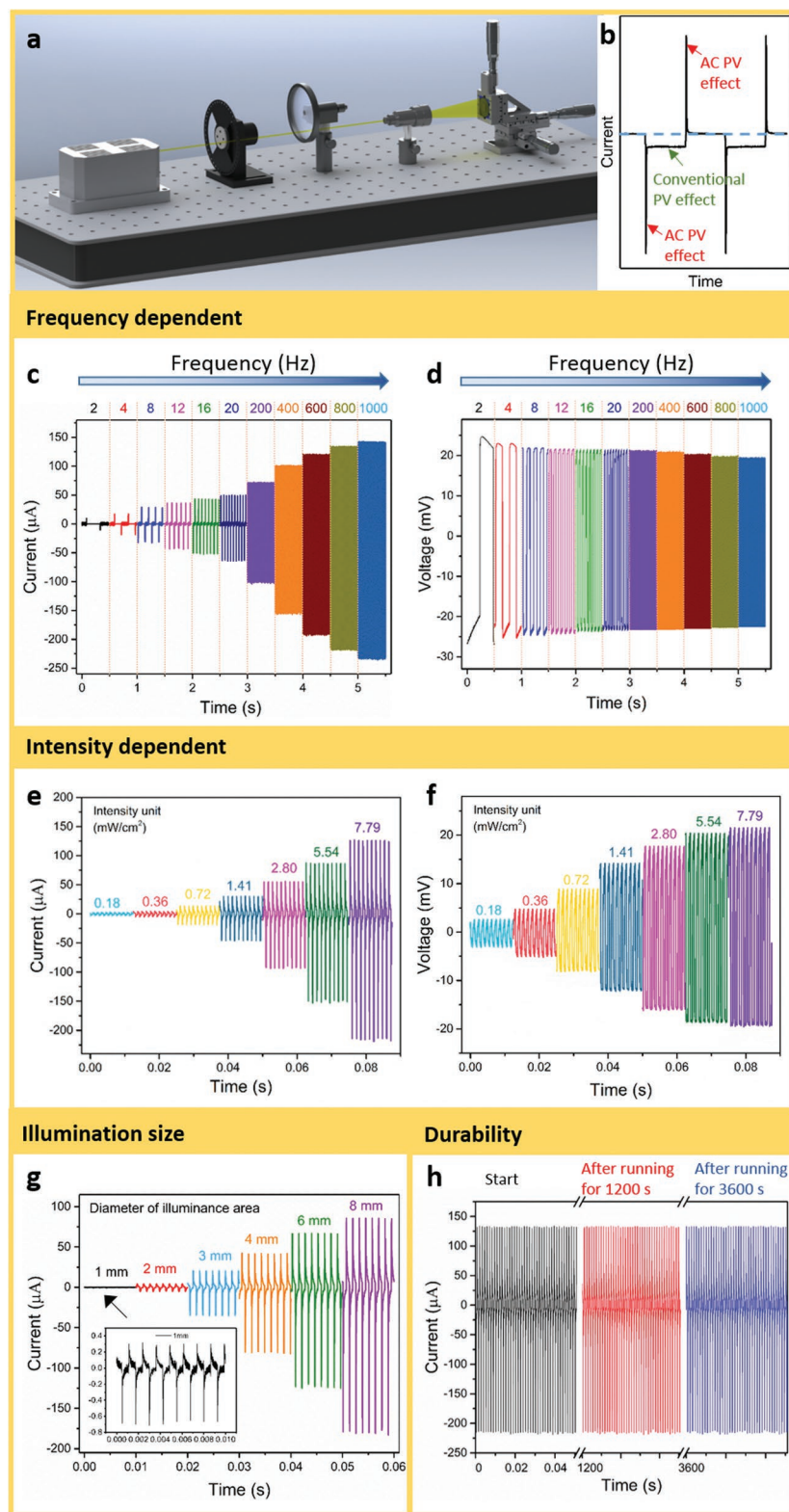
Here, by surprise, we find that except the DC output generated by the conventional PV effect, an alternating current (AC) is also produced if a light is incident upon the interface/junction of two materials periodically. When the device based on a p-Si/n-TiO₂ nanofilm was under the illumination of a flashing light at 442 nm with 7.79 mW cm⁻², the peak of the AC could reach 236 μA, and the peak of voltage of the AC output could reach more than 20 mV. This means that the observed current oscillates back and forth in the external circuit in responding to the flashing of light. This phenomenon is new and it cannot be explained by the established photovoltaic mechanisms in literature. The system is rather unique and different in the following aspects. In contrast to the conventional photovoltaic effect^[14] and thermoelectric effect,^[15] it generates an AC instead of DC. The device uses non-piezoelectric materials, the output characteristics are dissimilar to those of either piezoelectric effect for converting mechanical energy into electric power^[16,17] or pyroelectric effect.^[18,19] The device has no moving part in responding to direct mechanical triggering, so that the AC produced is not created by the triboelectric effect.^[20] Additionally, the AC does not follow the Ohm's law, instead it is based on Maxwell's displacement current model.^[21] From our experimental data, we have proposed a model to explain this newly founded phenomenon by suggesting a relative shift and realignment in quasi-Fermi levels for the materials adjacent to

Dr. H. Zou, Prof. G. Dai, A. C. Wang, Prof. X. Li, S. L. Zhang,
Prof. W. Ding, L. Zhang, Prof. Y. Zhang, Prof. Z. L. Wang
School of Materials Science and Engineering
Georgia Institute of Technology
Atlanta, GA 30332-0245, USA
E-mail: zhong.wang@mse.gatech.edu

Prof. Z. L. Wang
Beijing Institute of Nanoenergy and Nanosystems
Chinese Academy of Sciences
Beijing 100083, P. R. China

 The ORCID identification number(s) for the author(s) of this article can be found under <https://doi.org/10.1002/adma.201907249>.

DOI: 10.1002/adma.201907249



the junction/interface in response to the excitation and thermal effect of the illumination light under nonequilibrium conditions. This new effect provides a novel approach to detect a wide wavelength range of light, and it has ultrahigh sensitivity of light detection even at ultralow light intensity comparing to the conventional PV effect under the same conditions. The system could be also used as a remote wireless power source to boost the output of photocells for powering small-scale electronic devices. The devices are simple, low cost, easy fabrication, and could be easily integrated into silicon-based circuits.

Our first study is a device based on p-Si/TiO₂ nanofilm junction. A 15 nm thickness of TiO₂ was deposited on the pre-washed p-Si substrate via atomic layer deposition (ALD). The Al and indium tin oxide (ITO) are acted as the two electrodes at the p-Si and TiO₂ sides respectively. The active area of the device is about 0.8 cm × 0.8 cm. The measurement was set up under illumination of a 442 nm wavelength laser and an optical chopper was positioned to regulate the light switching on and off at a fixed frequency at (Figure 1a). An objective lens was used to expand the laser when necessary. Different from the conventional photovoltaic effect (Note S1, Supporting Information), it was operated at the nonequilibrium conditions and an appropriate filter setting is required. A high sampling rate is needed to record the signals, which is set as more than 10⁵ samples per second. As seen in Figure 1, when the chopper rotates, the device generates an AC. The Figure 1b shows that the typical signals from the device have AC components and DC components. Under the thermal equilibrium conditions that light is kept either on or off, there are two flat regions (DC current) in which the one close to 0 A is the dark current, and the other one is the photocurrent that is caused by the conventional photovoltaic effect. When the chopper rotating speed is high enough, the flat regions would be cut down due to the

under 442 nm illumination with 7.79 mW cm⁻² at different chopper frequencies (2–1000 Hz). e, f) Short-circuit current $I-t$ characteristics and open-circuit voltage $V-t$ characteristics of the p-Si/TiO₂ under 442 nm illumination with different power densities ranging from 0.18 to 7.79 mW cm⁻² at 800 Hz. g) $I-t$ characteristics of the p-Si/TiO₂ under 442 nm light with 7.79 mW cm⁻² with different illumination area (diameters range from 1 to 8 mm). h) The long-term durability and stability of the system under the 442 nm illumination of 7.79 mW cm⁻² at 1000 Hz. All measurements are carried out at zero bias.

short cycling time. The peaks of the AC are much higher than the output of the DC component. AC is produced only under the nonthermal equilibrium conditions that when the light is switched from off to on, the signal shows a trough followed with a flat photocurrent; when the light is switched from on to off, the output signal has a peak, then followed by a dark current. The current output value is strongly correlated to the chopper's rotating frequency. As shown in Figure 1c, with the increase of the working frequency from 2 to 1000 Hz, the negative short-circuit current I_{sc} rises from 10 to 236 μA . The negative current is superposition of two signals from both AC and DC, while the positive current is only from AC. Concerning the mechanism of this effect, the open-circuit voltage V_{oc} of the AC output was also measured by using the AC mode of a low-noise voltage preamplifier. Figure 1d shows that as the frequency increases, the V_{oc} of the AC output is relatively stable, despite a slightly declining trend that is seen from -27.1 to -22.5 mV. Figure 1c,d shows that as the frequency increase, the current increases while the voltage remained relatively unchanged. This is referred to as a capacitive conduction model^[21–24] rather than a resistive conduction model, in which the Maxwell's displacement current is the conduction mechanism for electricity transport (Note S2, Supporting Information). The experimental results demonstrate that the AC signals have strong dependent on light, the signals are not artificial facts (Note S3, Supporting Information). To approve this is not an artifact of the RC differentiator effect, waveforms that do not have discontinuous temporal derivatives in time (i.e., a sine wave or triangular wave) are also applied on the samples (Figure S1 and Note S3, Supporting Information). By integration of the current curve with respect to time, the total charges transferred in the AC part each cycle (from 2 to 800 Hz) remain almost the same which are about 22 nC, and only slightly decrease about $\approx 10\%$ at high-frequency rate (800–1000 Hz), this may because not all the charges are able to transfer in a short cycling time. It is notable that with increasing frequency, the time for the light to transit from completely on to fully off plummets initially and then gradually reduces at higher frequencies, as shown in Figure S2 (Supporting Information). By definition, current is the rate of flow of charge: $I = \frac{dQ}{dt}$. So, while the charges remain almost the same, a significantly shorter transit time leads a much larger current output. The relationship between current and voltage under various frequencies (Figure 1c,d) could also exclude the fact that the signals are from the RC differential effect (Notes S4 and S14, Supporting Information).

The magnitude of the current and voltage are also strongly related to light intensity. As the intensity increases from 0.18 to 7.79 mW cm^{-2} , the maximum current increases from -2.95 to -219 μA (Figure 1e) and the maximum voltage increases from -3.18 to -21.53 mV (Figure 1f) at a frequency of 800 Hz. This reveals that the electrical output is strongly associated with light absorption and the total amount of light excited charge carriers. This is further illustrated by the results in Figure 1g. Acrylic plates covered with aluminum foil were placed in front of the device. Holes ranging from 1 to 8 mm in diameter were cut by a laser cutter in the center of the acrylic plates to control the illumination area (Figure S3, Supporting Information). The beam was expanded, and the output was measured under the same illumination condition at 800 Hz. As the diameter increases

from 1 to 8 mm, the maximum current increases from -0.72 to -185 μA . The stability and repeatability studies are presented in Figure 1h. The device was subject to the working conditions for about 2 h with more than 3.6 million cycles, the output signals have no deviation nor degradation at all.

Not restricted to visible light of 442 nm wavelength, various wavelengths of lights are also able to produce the AC signals, as shown in Figure 2a1–a4. At different wavelengths of light ranging from ultraviolet (325 nm) to near-infrared (1060 nm) at a chopper rotating frequency of 1000 Hz, the device generates AC and the output values increase as the light intensity increases. With this effect, the device demonstrates a broadband response to a variety of light wavelengths, and the AC current is generated even when the exciting photon energy is below the bandgap (Figure S4, Supporting Information). The magnitude of the output under the illumination of various wavelength light is strongly associated with the light absorption of materials as shown in Figure 2a5 and Note S8 (Supporting Information).

The above-illustrated phenomenon is rather universal and has also been observed for other typical types of junctions, including Schottky contact (Al/p-Si/ITO), Ohmic contact (ITO/p-Si/ITO), metal–insulator–semiconductor (MIS, p-Si/AlO_x/ITO), and p–insulator–n (PIN, p-Si/AlO_x/ZnO). The details of the fabrication process are described in the Experimental Section and previous work.^[25] Briefly, a 200 nm thickness of Al and 100 nm of ITO were deposited as the electrodes via electron-beam evaporator and physical vapor deposition. The insulator layer AlO_x was deposited via ALD. Figure 2b1–e1 shows current–voltage characteristics of the junctions in dark and Figure 2b2–e2 shows current–time characteristics under the illumination of 442 nm light at a frequency of 20 Hz. These results reveal that this effect is universal and assuredly exists in a variety of junctions under the working conditions.

The observed phenomenon is undoubtedly a true effect. As demonstrated, the output current is highly dependent on the light intensity, the light absorption of materials, chopper frequency and illumination area. To further verify that the measured signals are indeed generated by the device, a number of “linear superposition” tests have been conducted (Figure 3 and Note S9, Supporting Information). The laser beam was expanded by an objective lens, and the intensity distribution of the laser beam followed a Gaussian distribution. Two p-Si/TiO₂ devices were placed at different positions with different light intensity so the electric output values are different. Both the short-circuit current (I_{sc}) and open-circuit voltage (V_{oc}) of each linear element device 1 and 2 (labeled as Dev 1 and Dev 2) were measured independently (Figure 3a,b,d,e). When the two electrodes of the devices are connected in reverse with the electrometer, the voltage and current pulses should be also reversed by reverting the sign. By comparing the results from experimental groups of Figure 3c1,c4, Figure 3c2,c3, Figure 3f1,f4, and Figure 3f2,f3, when two devices were connected in reverse to the measurement system, the output values of current and voltage were reversed respectively. The “switching polarity test” proves that the signals are from the devices themselves, since the signals would remain the same even when the polarity is switched if they come from noise or the environment. All eight

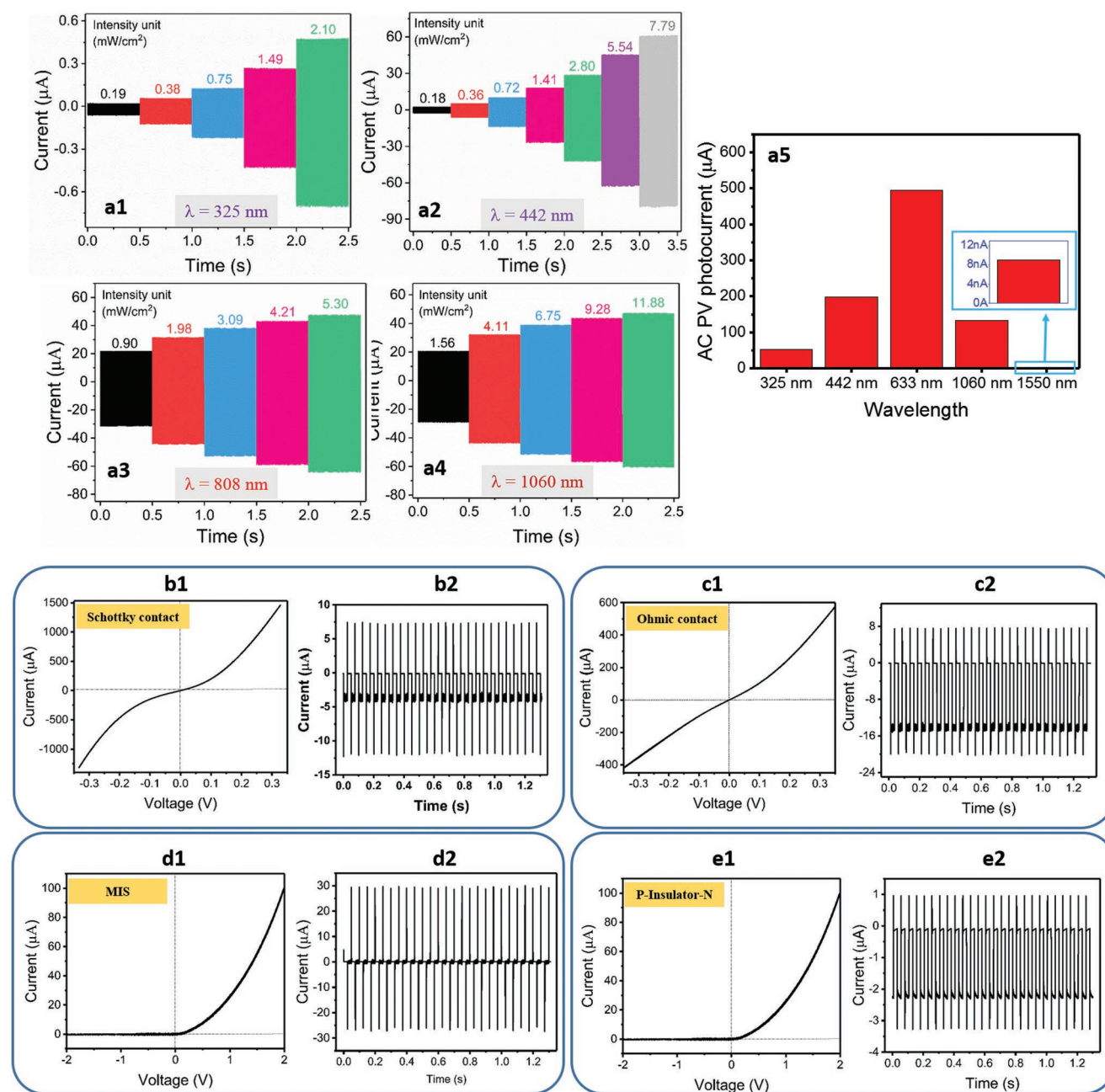


Figure 2. Feasibility and universality of this effect under various wavelengths of light and for different types of junctions. a1–a4) I - t characteristics of the junction of p-Si/n-ZnO nanowire arrays under the illumination with various wavelengths of light (325, 442, 808, 1060 nm), the chopper frequency is 1000 Hz. a5) Measured photocurrent under various wavelengths of light with intensity of about 2 mW cm^{-2} under zero bias at 1000 Hz. b1–e1) I - V characteristics of various junctions in the dark including Schottky contact (Al-pSi-ITO), Ohmic contact (ITO-pSi-ITO), metal-insulator-semiconductor (ITO- AlO_x -pSi), and p-insulator-n (pSi- AlO_x -ZnO nanowire arrays). b2–e2) I - t characteristics of various junctions under the 442 nm illumination with a power density of 7.79 mW cm^{-2} , the chopper frequency is 20 Hz. The I - t measurements are carried out at zero bias.

types of connection methods for two devices in both parallel and series models are illustrated in Figure 3. From the linearity theorem, when two devices are connected in parallel, the measured current equals the algebraic sum of the current response caused by each independent source; when in series, the measured voltage equals the sum of the voltage responses from the individual devices. The signal can be added up and subtract when they are in parallel (Figure 3c1,c4), antiparallel

(Figure 3c2,c3), in series (Figure 3f1,f4), and antiseriess (Figure 3f2,f3). The results satisfy the “switching-polarity” and “linear superposition” criteria and confirm that the electric output is indeed generated by the device.

Additional experiments were conducted to investigate the mechanism. When the flashing light is illuminated at the interface of two materials (point A), the AC current is generated (Figure 4a,b). However, when it is only illuminated at the

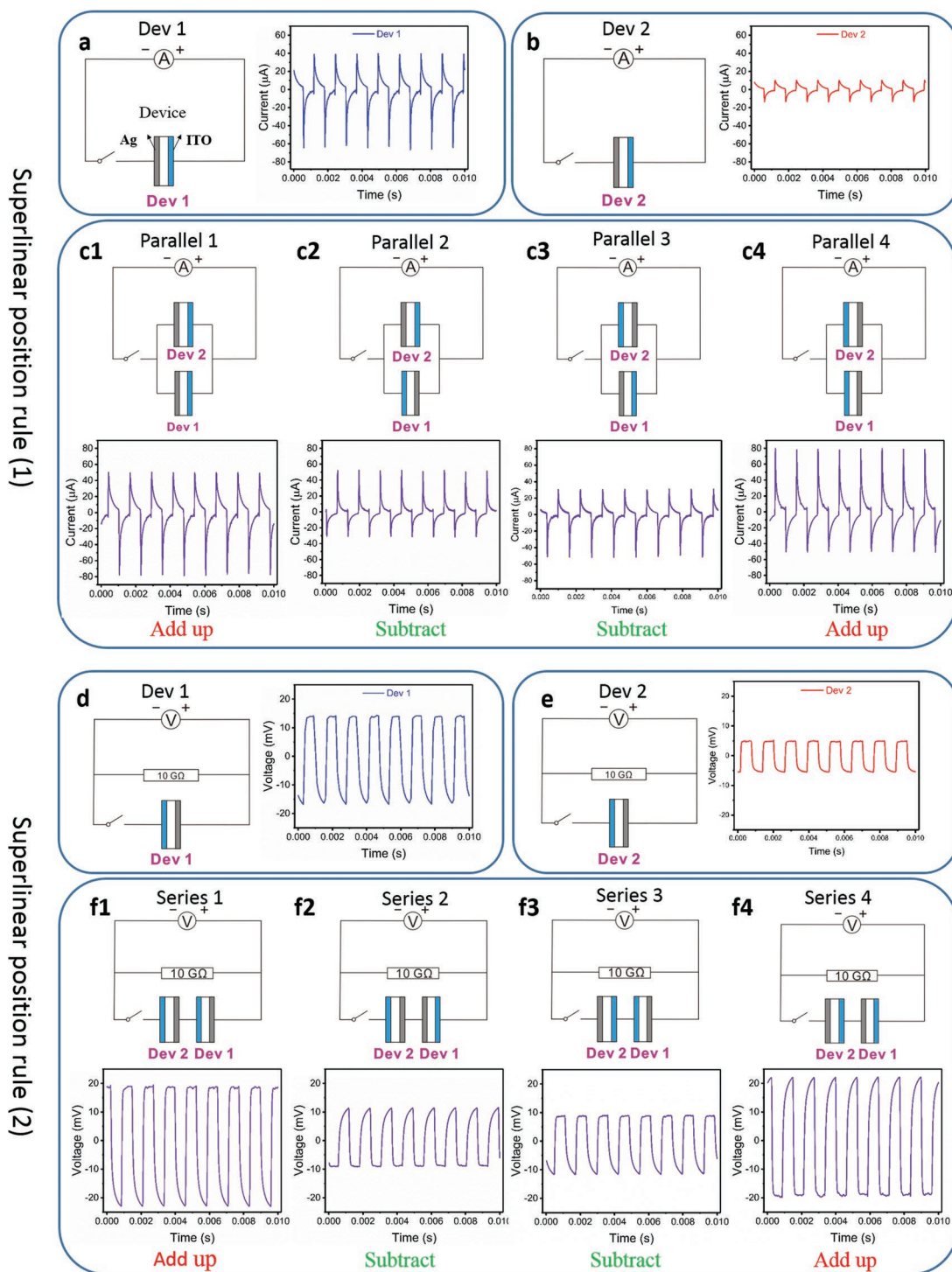


Figure 3. Linear superposition of current and voltage in different configurations. a,b) The connection schemes and $I-t$ characteristics two p-Si/TiO₂ devices Dev 1 (a) and Dev 2 (b) under the illumination of 442 nm light at 800 Hz. c1–c4) Four different configurations for two devices connected in parallels and their $I-t$ characteristics. d,e) The connection schemes and $V-t$ characteristics of two p-Si/TiO₂ devices Dev 1 (d) and Dev 2 (e) under the illumination of 442 nm light at 800 Hz. f1–f4) Four different configurations for two devices connected in series and their $V-t$ characteristics. All measurements are carried out at zero bias.

bulk p-Si (point B), there is no such AC signals (Figure 4c). The flashing light should be illuminated at the interface of two materials (Figure S7, Supporting Information), and at least one of two materials is semiconductor to generate excess carriers

(Note S11, Supporting Information). The effect is not caused by the concentration difference of excited carriers between the illuminated area and nonilluminated area (Dember effect, Notes S10 and S12, Supporting Information).

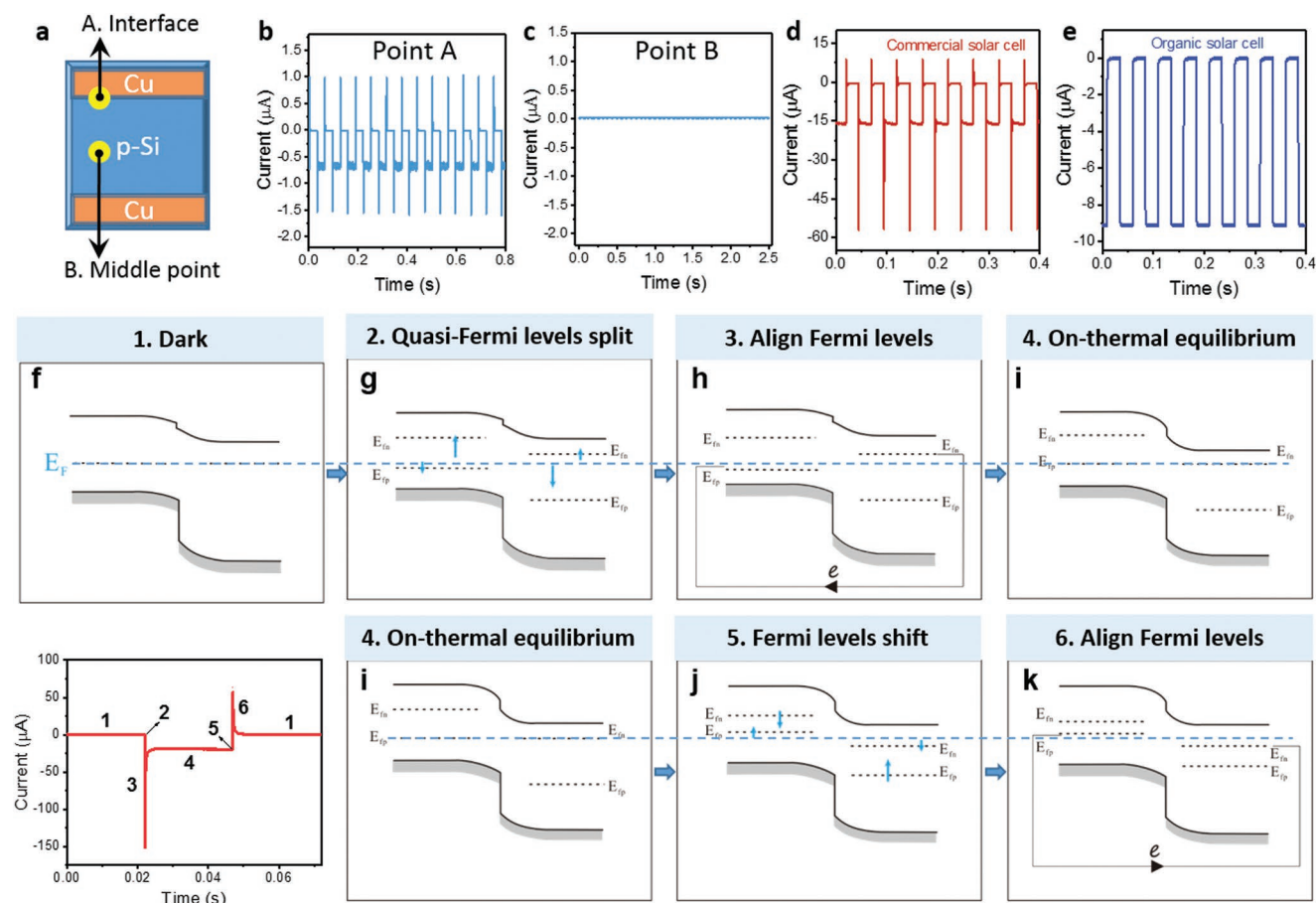


Figure 4. Proposed mechanism for the generation of alternating current in pn junction interfaces. a) Sketch map of the light positions on materials, either at the interface of two materials (point A), or in the middle between two electrodes (point B). b) $I-t$ characteristics of the device when the light point was located at the interface of two materials under the illumination of 442 nm laser with 6.8 mW cm^{-2} at 16 Hz. c) $I-t$ characteristics of the device when the light point was located in the middle under the same illumination condition. d) Output of a commercial solar cell under a green LED modulated with a function generator at a frequency of 20 Hz. e) Output of an organic solar cell measured at the same conditions as (d). f) Energy band diagram of a pn junction in the dark; the blue dotted line is the Fermi level E_F ; CB and VB are the conduction and valence bands. g) When the light is on, excess electrons and holes are generated, and the quasi-Fermi levels shift as described in the text. h) To balance the Fermi levels, a negative current peak was generated as a result of electrons flowing from the right electrode to the left electrode. i) Then, the Fermi levels are aligned at a new energy level (blue dotted line), the system reaches a new thermal equilibrium under the illumination. j) When the light is off, the quasi-Fermi levels shift reversely. k) A positive current peak was generated as the electrons flow back (from the left electrode to the right electrode) to balance the Fermi levels. And finally, the quasi-Fermi levels for electrons and holes coincide and the Fermi levels for p-type and n-type semiconductor are aligned again, returning to the original state in the dark (f).

Commercial silicon solar panels are based on p-n junction semiconductor, the AC output was also observed under the illumination of 642 nm laser (Figures S12 and S13, Supporting Information) in a commercial silicon solar cell (the technical details are shown in the Experimental Section). Bilayer organic photovoltaics are made of electron donor and acceptor heterojunction rather than semiconductor p-n junctions. Therefore an organic solar cell was fabricated,^[26] the performance details are shown in Figure S12 (Supporting Information). The active layer is poly(3-hexylthiophene) (P3HT):indene-C60 bis-adduct (ICBA) with a weight ratio of 1:1. No obvious AC was generated under the illumination of light from a green LED periodically in the organic solar cell, as shown in Figures S10 and S11 and Video S1 (Supporting Information). The result show that organic photovoltaics, which have no initial carrier concentrations (as p-type or n-type semiconductors), do not have the AC PV effect.

Based on the experimental results, theoretical discussion and analysis calculation, the possible mechanism is proposed. We take a pn junction device as an example. At the equilibrium status of the system in the dark, the concentrations of electrons, holes, and recombination center are stable, and they are determined by the Fermi levels and distribution functions (Figure 4f). The net carrier concentrations are constant and independent of time, the generation and recombination processes must be equal as follows

$$n_0 p_0 = n_i^2 = N_c N_v \exp\left(-\frac{E_g}{kT}\right) \quad (1)$$

where n_0 , p_0 are thermal equilibrium electron and hole concentrations that are independent of time, n_i is the intrinsic carrier density, N_c and N_v are the effective density of states in the

conduction band and valence band, E_g is the energy gap, k is the Boltzmann constant, and T is the temperature. From the equation of the Fermi level for thermal equilibrium, we have

$$E_F - E_{Fi} = kT \ln \left(\frac{n_0}{n_i} \right) \quad (2)$$

where E_F is the Fermi energy and E_{Fi} is the intrinsic Fermi energy.

When the light starts to shine on the semiconductor, it perturbs the original equilibrium conditions due to the light excitations. In this nonequilibrium condition, excess electrons Δn and holes Δp are created in pairs ($\Delta n = \Delta p$), and the carriers' generation rate is larger than the recombination rate, thus $np \neq n_0 p_0 = n_i^2$. At the time the injection is just introduced, the generation rate of electron-hole pair significantly increases, the recombination rate still remains the same at the beginning and start to grow.^[27,28] Carriers are generated faster than they recombine, the electrons and holes start to accumulate. This causes the imbalance of charges at two types of semiconductors. The quasi-Fermi levels can be determined by

$$E_{Fn} - E_F = kT \ln \left(1 + \frac{\Delta n}{n_0} \right) \quad (3)$$

$$E_F - E_{Fp} = kT \ln \left(1 + \frac{\Delta p}{p_0} \right) \quad (4)$$

where E_{Fn} , E_{Fp} are the quasi-Fermi energy levels for electrons and holes, respectively. The derivation is shown in Note S14 (Supporting Information). Equations (3) and (4) directly imply that if free electron-hole pairs are generated, E_{Fn} moves upward whereas E_{Fp} moves downward in the bandgap. The change of parameters during the whole processes are discussed in Note S15 (Supporting Information). For example, for a p-type ($p_0 \gg n_0$) at a low-injection condition ($\Delta p \ll p_0$), the quasi-Fermi level for holes E_{Fp} moves slightly closer to the valence band, the minority carrier-electron concentration increase significantly (n_0 is low), the quasi-Fermi energy level for electrons E_{Fn} deviates much from E_F and shifts up consequently toward the conduction band side.^[27] This is similar for an n-type semiconductor (Figure 4g). Due to sudden intervention or withdraw of light, the carrier density suddenly changes, the space charge distribution is disturbed, the Fermi levels are not at the same level. The shift of quasi-Fermi levels can be calculated as shown in Note S14 (Supporting Information). The balance is lost, the charge distribution between the two electrodes do not equal.

The deviation of quasi-Fermi energy levels from the Fermi level illustrates the deviation of the semiconductor from the thermal equilibrium state, and the greater their deviation, the more significant of the imbalance is. To balance the Fermi levels, as shown in Figure 4h, electrons will flow from the high to low E_F side through an external load until an equilibrium is reached, because the resistance of the barrier height is high enough to block the flow of electrons in reverse.^[17] In the capacitive model, the electrons accumulate at the interfacial region between the left electrode^[17,29,30] and the semiconductor

until the Fermi levels of the electrodes reach a new equilibrium value (Figure 4i). When excess carriers are generated, the conductance of the semiconductor significantly increases and the induced potential is proportional to the amount of excess carriers excited, so the current increases significantly.^[28] From Equations (3) and (4), higher intensity of light generates more electron-hole pairs, and the deviation of quasi-Fermi levels and the imbalance of charge distribution are more significant, more charges are transferred between electrodes, which leads to a higher current, as shown in Figures 1 and 2.

After a period of illumination, the concentrations of excess electrons and holes in the system reach a steady-state, and the generation rate and recombination rate are equal and independent of time. Under this new equilibrium state, in short-circuit condition, only DC current by photovoltaic effect is generated under the light, and the E_{Fp} for p-type and the E_{Fn} for n-type are at the same level,^[5] and closer to the valence band in the p-type semiconductor (Figure 4i).

When the light is turned off, at first, the generation rate of the light-induced excessive carriers decrease immediately, but the recombination rate remains the same.^[28] The electrons will gradually fall down to the valence band and recombine with holes; during this process, the recombination rate of charge carriers is greater than the generation rate. As the concentration of holes and electrons are decreasing below this new thermal equilibrium value, the recombination rate starts to decrease, and finally the system returns to the initial dark thermal-equilibrium state when the recombination rate equals the generation rate. For the p-type semiconductor, the quasi-Fermi level for holes E_{Fp} moves slightly away from the valence band; the minority carrier-electron concentration has decreased significantly relatively, and consequently, the quasi-Fermi energy level for electrons E_{Fn} shifts down. The n-type semiconductor behaves in a similar manner (Figure 5j). To align the Fermi levels, the electrons that had accumulated near the left electrode flow back through the external circuit to the right electrode (Figure 5k), as the reverse direction of electrons flow is blocked by the contact barrier,^[17] returning the system to its original state. The excess electron-hole pairs disappear, and the concentrations of electrons and holes have to decrease to the original value in dark. Finally, the semiconductor returns to the initial thermal equilibrium state in dark as well as the thermal equilibrium Fermi level (Figure 5f).

Different from the conventional PV effect, the AC PV effect involves 4 states (Note S15, Supporting Information), and six physical processes (Figure 4a-f), and it follows the displacement current model. The conventional PV effect is driven by the electric field in the depletion regions, that holes flowing to the p-side and electron flowing to the n-side; here, in the AC PV effect, the excessive charge carriers excited by the light or other facts, causing Fermi levels shift and the imbalance of charge distribution, which will drive the electrons to flow to level the Fermi levels and balance the potential difference at the transition states. The details of the comparison of the two effects are discussed in Note S16 (Supporting Information). To create the nonthermal equilibrium states, it requires external changing fields, like light, electricity, or magnetic field or others, which can be driven by an external mechanical power. Hence, the driven force mainly comes from these power sources that cause

the redistribution of charges to balance the Fermi levels. Obviously, when the external mechanical power stops, the carrier concentration gradually reaches a steady-state value, the electrons and holes have no accumulation or degradation over time, the equilibrium state occurs when the Fermi energy levels are the same in the two materials.

The surface energy levels within the bandgap would be another effect that contributes to the mechanism (Note S17, Supporting Information). The interband absorption of light for Silicon is below 1100 nm, but when the 1545 nm light was illuminated at the junction, the photocurrent was observed as well (Figure S4, Supporting Information). This demonstrates that the silicon has surface energy states. When the system is in a state of thermal equilibrium, there are no excess carriers and no Fermi level shift, and the surface energy levels are in a steady-state. When the light turns on, a relative shift of quasi-Fermi levels may cause a significant amount of charges to be transferred and/or redistributed within the surface and/or the bulk. The empty surface energy levels of materials could store electrons and then are negatively charged, and/or lose electrons and positively charged, which results in a potential difference between electrodes to drive the current flow through the external circuit to balance the charges.^[17] When the light turns off, in this nonthermal equilibrium, the Fermi levels shift back, the excess carriers gradually disappear, and the neutralized energy levels lose electrons and become positively charged. This drives the current flow in the opposite direction to return to the initial state. The surface energy states have the ability to store electrons,^[27,28,31,32] which would clarify the capacitive model. The external voltage could shift the Fermi levels and change the surface states, therefore if the voltage is high enough, surface states are not able to trap or release the electrons (Note 18, Supporting Information).

The excess carriers can be induced not only by light, but also by transient electric or other energy transmission methods,^[28] which can also break the equilibrium condition. Here we demonstrate that when a metal probe contacts a semiconductor, it injects excess carriers into the device, the same effect is observed as well (Note 19, Supporting Information).

This effect can have many practical applications, such as active sensors and power sources. Broadband photodetectors have extensive applications in communication systems, medical and thermal imaging, environmental monitoring, and defense technology. For such applications, the photodetectors must satisfy stringent requirements such as high sensitivity at operating wavelengths, high response speed, and minimum noise. The principle of the traditional photodiode is the interband absorption of light in the depletion layer of the diode and the subsequent separation of electrons and holes by the electric field. An external voltage bias is always applied to strengthen the internal electric field; however, this will lead to a large dark current and require external power to drive the device. By using this effect, the fabricated device demonstrated outstanding performance as a photodetector with ultrahigh sensitivity, ultralow noise and good response speed. **Figure 5a** shows a typical $I-t$ characteristic of the PD based on p-Si/TiO₂ nanofilm at zero voltage under the illumination of 442 nm light with an intensity of ≈ 7 mW cm⁻² at a frequency of 1000 Hz. The output is an AC, which is different from the output from a pn photodiode

based on the conventional photoelectric effect. To measure the linearity and sensitivity, this PD was measured under various intensity. The dark current could be as low as 0.9 nA. The sensitivity defined as $(I_{\text{light}} - I_{\text{dark}})/I_{\text{dark}}$ is found to be $2.09 \times 10^7\%$ at 7.79 mW cm⁻² via this effect, which could be about 200 times larger than that of the same device based on the photovoltaic at -2 V bias, and more than 2051 times larger than that via photovoltaic effect without bias (Figure 5b). Even at ultralow intensities of 3, and 6 $\mu\text{W cm}^{-2}$, the sensitivities are as high as 934%, and 4250%, while the output based on photovoltaic effect does not exhibit obvious signals at all. Higher sensitivities will enable higher signal levels and leads to more accurate results. As demonstrated, the devices have distinct advantages: operation without bias, ultrahigh sensitivity even at ultralow intensity, ultrafast response time (as low as ≈ 20 μs , as shown in Notes 20 and 21, Supporting Information), and broadband response to a wide range of wavelengths from the ultraviolet to near-infrared light (Figure 2).

Aside from sensor applications, it can also work as a power source for small scale devices. Energy densities were investigated by connecting it in series with external variable resistors under the 442 nm light illumination of 7.79 mW cm⁻², at a fixed chopper frequency of 1000 Hz. Apparently, the current decreases with the increment of resistance from 1 Ω to 1 M Ω , and the power densities increase sharply first, and are subsequently saturated when the load resistance is increased to 400 Ω , but diminishes to nearly zero when the resistance is increased to 1 M Ω (Figure 5c,d). The maximum current density is 347 $\mu\text{A cm}^{-2}$, and the power density, the amount of power per unit volume, is as high as 103 Wh L⁻¹, which is comparable to the energy density of lead-acid and Ni-Cd batteries.^[33]

A commercial capacitor could be charged by the output from the device when it was working under a periodical illumination (Figure 5f). We connected the device to a transformer and a rectifier first, and then connected it to a capacitor with a capacitance of 0.15 μF . The capacitor was fully charged in about 10 s. The short-circuit transferred charges in the AC regions are calculated by integration, and it is around 22 nC per single peak cycle. Since the frequency can be easily modulated to a high value as compared to other direct physical contact modes,^[17,34-36] the total charges transferred could be large per unit of time, and therefore the capacitor charging process would be very fast. In addition, a mini commercial solar panel was also used to demonstrate the application of this effect in boosting the output of the photocells. The electric output of the device was studied under the illumination of 642 nm monochromatic laser. The laser beam is expanded with a diameter of about 1 cm and follows the Gaussian distribution. By the conventional PV effect, the open-circuit voltage (V_{oc}) and short-circuit current (I_{sc}) of the commercial solar panel were measured to be ≈ 1.29 V, and 8 μA , respectively. Via the alternating current photovoltaic (AC PV) effect, the same device has a maximum V_{oc} of 1.32 V, and a maximum I_{sc} of 219 μA (Figure 5g). The electric output of the device under different external loads was further studied under the same illumination conditions. The device was connected with different resistors from 10 Ω to 22 M Ω . As displayed in Figure S18 (Supporting Information), all the current amplitudes drop with increasing load resistances owing to ohmic loss, whereas the voltages follow a reverse trend. As a

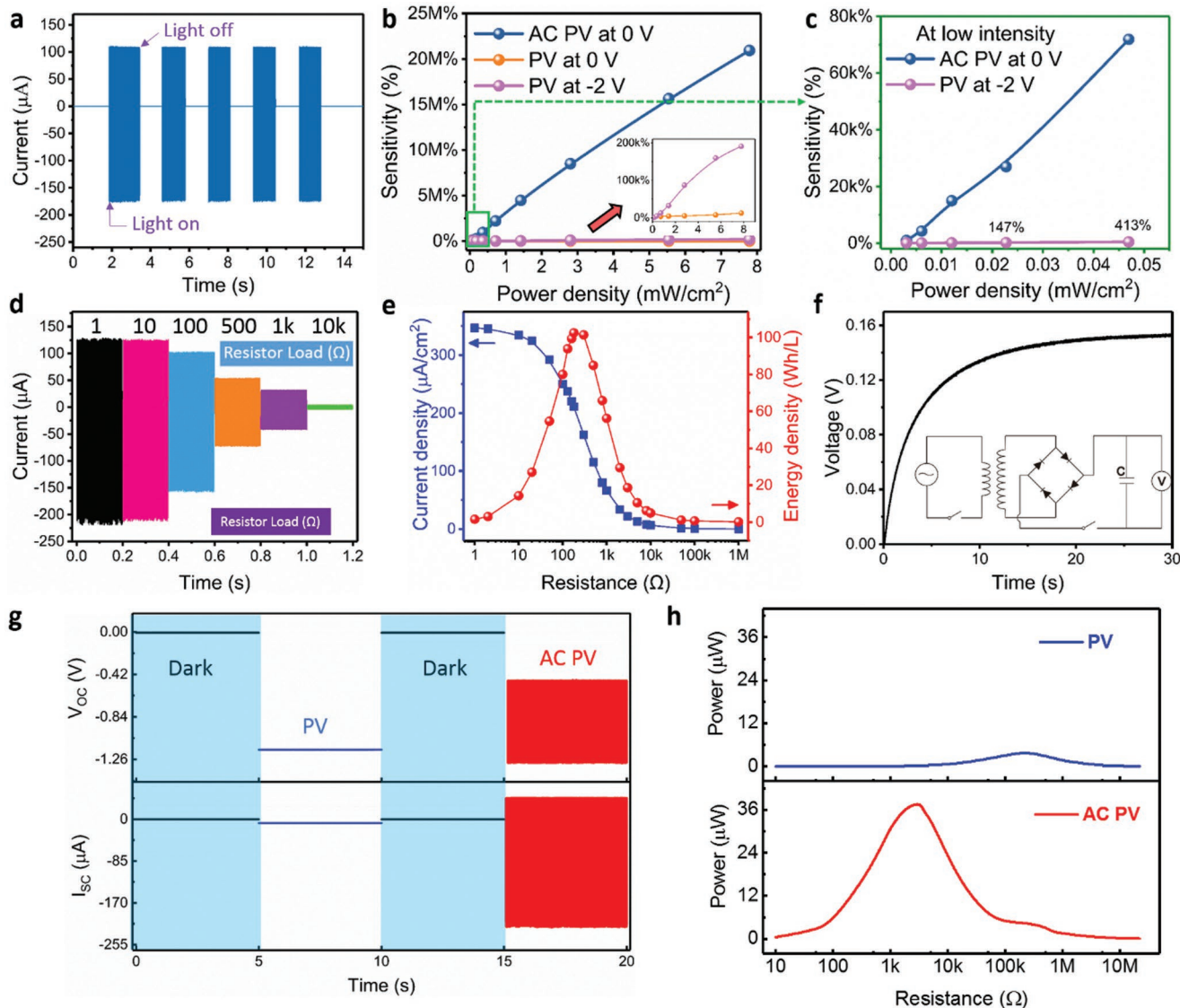


Figure 5. The demonstration of applications of the effect as a sensor and a power source. a–c) Electrical output of the photodetector (PD) based on p-Si/TiO₂ via this new effect. a) Typical electrical output of PD based on this effect. b) The corresponding sensitivity of the device based on this effect under different illumination power densities compared to the value from the conventional photovoltaic effect. c) The corresponding sensitivity of the device under the ultralow light intensities. d–f) Electrical output of the power source based on p-Si/TiO₂ via this new effect. The device is connected with various resistors without voltage bias. d) *I*–*t* characteristics of the device under the illumination of 442 nm light at frequency of 800 Hz. e) Current density (blue points and line) and energy density (red points and line) with different external load resistances varying from 1 Ω to 1 MΩ. f) Charging curve of a capacitor charged by AC output from the device via this new effect under the illumination of 442 nm laser at 1000 Hz. The inset shows the circuit diagram. g, h) Electrical output of a commercial silicon solar cell panel under the illumination of 642 nm laser with 11.10 mW cm⁻². g) Open-circuit voltage *V*_{oc} and short-circuit current *I*_{sc} in dark (black line), constant illumination (blue line), and flashing light at 1000 Hz (red line). h) Dependence of the output power of the solar cell on the load resistances. The top panel shows the power output when the device is under continuous illumination. The bottom panel shows the output under laser illumination with a chopper frequency of 1000 Hz.

result, the instantaneous peak power is maximized at matched load resistances. The commercial solar panel is capable of stably delivering a maximum output power of 3.77 μW with a load of 200 k Ω, while by utilizing the AC PV effect, it could reach 4.49 μW at the same load. However, the maximum power output could reach up to 37.63 μW with a load of 2 k Ω provided by AC PV effect, about 11.2 times larger than the maximum output provided by the conventional photovoltaic effect (Figure 5h). Consequently, via the AC PV effect, the output

power evidently enhanced compared to that of conventional PV effect, which would be an improvement in using the devices as a power source.

The long-term durability of the power knit has been shown in Figure 1f, where there is no decrease after millions of cycles, clearly demonstrating the practical value of this stable and reliable AC electric power source. The noncontact mode of operation has no friction between materials, so there would be no material's wearing, leading to high durability. As the laser has

a good spatial coherence, the power delivered by the laser has less energy loss in the light transfer process, and could avoid the limitations and hassle of electric wires to function as a remote wireless power supply system. The output power of the system can be adjusted precisely and easily by various methods, including light intensity, switching frequency or illumination area. Overall, the utility model has great potential application in sensing for human-machine interfaces, environmental monitoring, and security. It has the advantages of a simple structure, easy fabrication and assembly, low cost and small volume size. The laser light working as a power source, it can transport energy via vacuum or harsh environments that humans cannot access, and the devices could be used as sustainable remote wireless power sources. We believe the further improvement on the output and the large-scale integration technologies would make them suitable for large devices and electrical appliances.

In summary, a new type of photovoltaic effect has been discovered that an AC electric power is generated at the transition states when the light periodically illuminated at the interface of materials. The effect is strongly affected by the light intensity, switching frequency, and illumination area and is truly universal since it exists for various types of junctions under a wide range of wavelengths. Additionally, the system operates in nondirect contact mode and has excellent long-term durability. The effect is likely due to a relative shift and realignment between the quasi-Fermi levels of the semiconductors adjacent to the junction/interface under the nonequilibrium conditions, which results in electron flow in the external circuit to balance the potential difference between the electrodes. It could have a significantly higher current output than that from DC output via the photovoltaic effect. Using the new effect, the device that could work as an active photodetector that has a significantly higher current than that produced by conventional PV effect, and ultralow dark current without a voltage bias, resulting in an ultrahigh sensitivity even at an ultralow light intensity. Additionally, with the new effect, it could boost the power output from photocells. Our study opens a valuable route for improving the performance of optoelectronic devices.

Experimental Section

Fabrication Process of the Devices: p-Type Si wafers (B-doped (100) wafer, 1–10 Ω cm, UniversityWafer Inc.) were washed by ultrasonicator with acetone, isopropyl alcohol, and distilled water respectively for 20 min. The wafers were cut into pieces by dicing saw, each piece had a size of 1 cm \times 1 cm. The devices with different junctions were processed via E-beam evaporator, physical vapor deposition (PVD), radio frequency (RF) sputter, and ALD. TiO_2 , AlO_x with a thickness of 15 nm was coated by Cambridge NanoTech Plasma ALD. ITO was deposited by PVD75 RF Sputterer, Kurt J. Lesker Company. The thickness of the ITO layer was about 100 nm. Cr and Al were deposited by Denton Explorer E-beam evaporator with a thickness of 200 nm.

Commercial Solar Panel: The mini solar panel was purchased from Sundance Solar Inc., the item model number was 700-10850-28. According to the information for the vendor, the miniature solar panel had an efficiency of 16.0%, an open-circuit voltage of 6 V, and a short-circuit current of 55 mA, with a peak voltage of 5.0 V, and peak current of 50 mA. The dimensions were 75 mm (L) \times 29 mm (W) \times 3 mm (D).

Fabrication of ZnO Nanowires: ZnO seed layer was deposited by RF magnetron sputtering (PVD RF75, Kurt J. Lesker Company) with a thickness of about 100 nm. The coated samples were then placed

into mixed growth solution (25×10^{-3} M $\text{Zn}(\text{NO}_3)_2$, 12.5×10^{-3} M hexamethylenetetramine, and 0.8 M ammonium hydroxide) in a mechanical convection oven (Yamato DKN400, Santa Clara, CA, USA) at 95 $^\circ\text{C}$ for 90 min. The samples were washed with isopropyl alcohol and distilled water, and dried in the oven at 60 $^\circ\text{C}$ for several hours. Poly(methyl methacrylate) (MicroChem 495PMMA A8) was spin coated onto the samples, and then the samples were treated with oxygen plasma by reactive ion etching (Vision RIE) for 4 min to expose the tips of ZnO nanowires. A thin layer of ITO was deposited on ZnO as the top electrode and Al was deposited on p-Si as the bottom electrode. Samples then were cleaned with acetone to remove the PMMA layer, and fired at 350 $^\circ\text{C}$ for 2 h in a compact rapid thermal processing tube furnace (RTP-1000D4, MTI Corporation). Testing wires were connected to the electrodes by silver paste.

Fabrication of Organic Solar Cell: For organic solar cell devices, glass substrates coated with ITO were coated with PEIE (10 nm) and worked as the electron-collecting electrodes. The active layer was P3HT (4002-E, BJ19-98, Rieke Metals): ICBA (Lumtec) with a weight ratio of 1:1. The 40 mg mL^{-1} chlorobenzene solutions were first filtered through a 0.2 mm pore PTFE filter, and spin-coated at a speed of 1000 rpm with an acceleration of 10 000 rpm s^{-1} . The fabricated devices were annealed at 160 $^\circ\text{C}$ for 10 min in a glove box. 15 nm MoO_3 and 150 nm of Ag were then deposited through a shadow by an e-beam evaporator. The active area size was 4 mm^2 .

Measurements: I - V characteristics of the devices were measured and recorded by a computer-controlled measurement system with a Stanford SRS low noise current preamplifier (SR570)/SRS low noise voltage preamplifier (SR560) in conjunction with a GPIB controller (GPIB-USB-HS, NI 488.2). The data were measured without filter, and the sampling rate was set to be more than 10^5 s^{-1} . I - t characteristics of the devices were measured by the current preamplifier (SR570) without filter at zero bias. V - t characteristics of the p-Si/ TiO_2 device was measured by the low noise voltage preamplifier (SR560) and Keithley 6514 electrometer. The sample rate was set as 10^5 samples s^{-1} . The optical input stimuli were provided by a He-Cd laser (wavelength = 442 nm, model no. KI57511-G, Kimmon Koha Co., Ltd.). A continuously variable filter was used to control the light power density, which was measured by a thermopile power meter (Newport 818P-001-12).

Supporting Information

Supporting Information is available from the Wiley Online Library or from the author.

Acknowledgements

The authors thank Prof. Bernard J. Kippelen and Dr. Canek Fuentes-Hernandez for constructive discussions and guidance on fabricating organic solar cells. The authors thank Prof. John Reynolds, Ian Pelse, and Gus Lang for providing the help on measuring the performance of devices. This work was financially supported by the U.S. Department of Energy, Office of Basic Energy Sciences (Award DE-FG02-07ER46394) (the device fabrication and measurements) and the National Science Foundation (DMR-1505319) (materials synthesis and application in sensors).

Conflict of Interest

The authors declare no conflict of interest.

Author Contributions

Z.L.W. supervised and guided the project; H.Z. conceived and designed the study, fabricated the devices; H.Z., G.D., A.C.W., X.L., and S.Z.

performed the experiments; H.Z. and W.D. set up the measurement; H.Z., Z.L.W., A.C.W., S.Z., and Y.Z. prepared the manuscript with input from all authors.

Keywords

AC photovoltaic effect, alternating current, excessive carriers, nonthermal equilibrium state, photovoltaic effect, quasi-Fermi levels

Received: November 4, 2019

Revised: January 2, 2020

Published online:

- [1] H. Y. Zou, J. Chen, Y. N. Fang, J. L. Ding, W. B. Peng, R. Y. Liu, *Nano Energy* **2016**, 27, 619.
- [2] J. Chen, Y. Huang, N. N. Zhang, H. Y. Zou, R. Y. Liu, C. Y. Tao, X. Fan, Z. L. Wang, *Nat. Energy* **2016**, 1, 16138.
- [3] M. A. Green, Y. Hishikawa, E. D. Dunlop, D. H. Levi, J. Hohl-Ebinger, A. W. Y. Ho-Baillie, *Prog. Photovoltaics* **2018**, 26, 3.
- [4] S. M. Sze, K. K. Ng, *Physics of Semiconductor Devices*, John Wiley & Sons, Hoboken **2006**.
- [5] M. A. Green, *Solar Cells: Operating Principles, Technology and System Applications*, University of New South Wales, Kensington, Australia **1992**.
- [6] B. Oregan, M. Gratzel, *Nature* **1991**, 353, 737.
- [7] Y. G. Gurevich, A. V. Meriuts, *Phys. Lett. A* **2013**, 377, 2673.
- [8] J. Frenkel, *Nature* **1933**, 132, 312.
- [9] A. G. Chynoweth, *Phys. Rev.* **1956**, 102, 705.
- [10] P. J. Sturman, *Photovoltaic and Photo-refractive Effects in Noncentrosymmetric Materials*, Vol. 8, CRC Press, Boca Raton, FL, USA **1992**.
- [11] A. M. Danishevskii, A. A. Kastalsk, S. M. Ryvkin, I. D. Yaroshetskii, *Sov. Phys. - JETP* **1970**, 31, 292.
- [12] I. Brevik, *Phys. Rep.* **1979**, 52, 133.
- [13] W. W. Anderson, Y. G. Chai, *Energy Convers.* **1976**, 15, 85.
- [14] M. Grätzel, *Nature* **2001**, 414, 338.
- [15] J. R. Sootsman, D. Y. Chung, M. G. Kanatzidis, *Angew. Chem., Int. Ed.* **2009**, 48, 8616.
- [16] Z. L. Wang, J. H. Song, *Science* **2006**, 312, 242.
- [17] R. S. Yang, Y. Qin, L. M. Dai, Z. L. Wang, *Nat. Nanotechnol.* **2009**, 4, 34.
- [18] C. R. Bowen, J. Taylor, E. LeBoulbar, D. Zabek, A. Chauhan, R. Vaish, *Energy Environ. Sci.* **2014**, 7, 3836.
- [19] Y. Yang, W. X. Guo, K. C. Pradel, G. Zhu, Y. S. Zhou, Y. Zhang, Y. F. Hu, L. Lin, Z. L. Wang, *Nano Lett.* **2012**, 12, 2833.
- [20] J. Chen, Y. Huang, N. Zhang, H. Zou, R. Liu, C. Tao, X. Fan, Z. L. Wang, *Nat. Energy* **2016**, 1, 16138.
- [21] J. C. Maxwell, *The London, Edinburgh and Dublin Philosophical Magazine and Journal of Science*, Taylor & Francis, London, UK **1862**.
- [22] Z. L. Wang, *Mater. Today* **2017**, 20, 74.
- [23] J. D. Jackson, *Classical Electrodynamics*, Wiley, New York **1975**.
- [24] Z. L. Wang, A. C. Wang, *Mater. Today* **2019**, 30, 34.
- [25] H. Zou, X. Li, W. Peng, W. Wu, R. Yu, C. Wu, W. Ding, F. Hu, R. Liu, Y. Zi, Z. L. Wang, *Adv. Mater.* **2017**, 29, 1701412.
- [26] Y. H. Zhou, C. Fuentes-Hernandez, J. Shim, J. Meyer, A. J. Giordano, H. Li, P. Winget, T. Papadopoulos, H. Cheun, J. Kim, M. Fenoll, A. Dindar, W. Haske, E. Najafabadi, T. M. Khan, H. Sojoudi, S. Barlow, S. Graham, J. L. Bredas, S. R. Marder, A. Kahn, B. Kippelen, *Science* **2012**, 336, 327.
- [27] D. A. Neaman, *Semiconductor Physics and Devices*, Irwin, Chicago, IL, USA **1992**.
- [28] E. K. Liu, B. S. Zhu, J. S. Luo, *Semiconductor Physics*, Publishing House of Electronics Industry, Beijing, China **2011**.
- [29] Z. L. Wang, *Mater. Today* **2017**, 20, 74.
- [30] H. Y. Zou, Y. Zhang, L. T. Guo, P. H. Wang, X. He, G. Z. Dai, H. W. Zheng, C. Y. Chen, A. C. Wang, C. Xu, Z. L. Wang, *Nat. Commun.* **2019**, 10, 1427.
- [31] D. S. Campbell, *Capacitive and Resistive Electronic Components*, Vol. 8, CRC Press, Boca Raton, FL, USA **1994**.
- [32] R. F. Pierret, *Semiconductor Device Fundamentals*, Addison-Wesley, Reading, MA, USA **1996**.
- [33] J. M. Tarascon, M. Armand, *Nature* **2001**, 414, 359.
- [34] K. Dong, J. Deng, Y. Zi, Y. C. Wang, C. Xu, H. Zou, W. Ding, Y. Dai, B. Gu, B. Sun, Z. L. Wang, *Adv. Mater.* **2017**, 29, 1702648.
- [35] J. Chen, S. K. Oh, H. Y. Zou, S. Shervin, W. J. Wang, S. Pouladi, Y. L. Zi, Z. L. Wang, J. H. Ryou, *ACS Appl. Mater. Interfaces* **2018**, 10, 12839.
- [36] C. Xu, Y. L. Zi, A. C. Wang, H. Y. Zou, Y. J. Dai, X. He, P. H. Wang, Y. C. Wang, P. Z. Feng, D. W. Li, Z. L. Wang, *Adv. Mater.* **2018**, 30, 1706790.